Environmental Science & Technology

Article

Cite This: Environ. Sci. Technol. 2019, 53, 1947−1957

pubs.acs.org/est

Domestic and Transboundary Sources of Atmospheric Particulate Bound Mercury in Remote Areas of China: Evidence from Mercury Isotopes

Xuewu Fu,*,† Hui Zhang,† Xinbin Feng,*,† Qingyou Tan,† Lili Ming,‡ Chen Liu,† and Leiming Zhang§

†State Key Laboratory of Environmental Geochemistry, Institute of Geochemistry, Chinese Academy of Sciences, 99 Lincheng West Road, Guiyang, 550081, China

‡Department of Civil and Environmental Engineering, The Hong Kong Polytechnic University, HungHom, Kowloon, Hong Kong

§Air Quality Research Division, Science and Technology Branch, Environment and Climate Change Canada, Burlington, Ontario L7S 1A1, Canada

Supporting Information

ABSTRACT: Isotopic composition of atmospheric particulate bound mercury (PBM) was obtained at four remote sites in different geographical regions of China for three to 12 month periods. Mean ($\pm 1\sigma$) $\Delta^{199}Hg_{PBM}$ was the highest at the site in southwestern China (0.66 ± 0.32‰), followed by the site in northeastern China (0.36 ± 0.34‰), the site in the marine boundary layer of East China Sea (0.35 ± 0.33‰), and was the lowest at the site in northwestern China (0.27 ± 0.22‰). $\Delta^{199}Hg_{PBM}$ was relatively higher in cold than warm season at the sites in northwestern and southwestern China, whereas the opposite was found at the site in northeastern China. We propose that the seasonal variations of $\Delta^{199}Hg_{PBM}$ were influenced by the exposure of air masses to regional (e.g., anthropogenic and dust related) and long-range (e.g., anthropogenic and oceanic) sources in the preceding several days, with the former characterized by lower $\Delta^{199}Hg_{PBM}$ and the latter characterized by more positive $\Delta^{199}Hg_{PBM}$ due to sufficient atmospheric transformations. Modeling results from Potential Source Contribution Function suggested that domestic anthropogenic emission was the major contributor to PBM pollution at the sites in northeastern and eastern China, whereas long-range transboundary transport of PBM from South Asia played a more important role at the sites in southwestern and northwestern China.

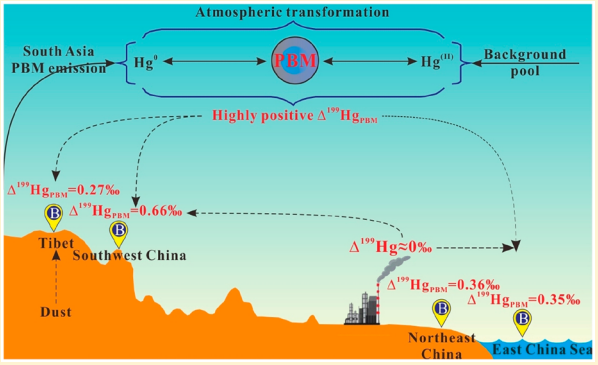

1. INTRODUCTION

Mercury (Hg) stable isotope analysis is a useful tool in identifying Hg sources and transformation mechanisms. Hg has seven stable isotopes (Hg^{196}, Hg^{198}, Hg^{199}, Hg^{200}, Hg^{201}, Hg^{202}, and Hg^{204}). Significant advances have been made in measuring Hg isotopes in the natural environments during the past decade.[1,2] Mass-dependent fractionation (MDF) and mass-independent fraction (MIF) of Hg isotopes were observed in geogenic and biological materials.[1] MDF of Hg isotopes could be induced by many natural processes including reduction/oxidation, methylation/demethylation, sorption, evaporation, and volatilization,[3−11] whereas significant MIF of Hg isotopes are mainly triggered by photochemical reactions.[3,6,12,13]

Gaseous elemental mercury (GEM), particulate bound mercury (PBM), and gaseous oxidized mercury (GOM) are the three operationally defined forms of Hg in the atmosphere. Recently, measurements of total gaseous mercury (TGM = GEM + GOM) or GEM isotopic compositions were conducted in United States, Europe, and East Asia.[5,14−21] These studies observed distinguishable MDF ($\delta^{202}Hg$) and MIF ($\Delta^{199}Hg$ and $\Delta^{201}Hg$) signatures of TGM or GEM between background atmospheric pool and anthropogenic sources, providing a useful clue to identify the sources and atmospheric transformations of Hg.[14,16,17]

PBM in the atmosphere could be derived from direct anthropogenic sources or produced via atmospheric transformations, and depleted by photoreduction or deposition. Modeling studies assumed atmospheric transformations between PBM and other Hg species in the atmosphere to be the dominant factor influencing atmospheric PBM.[22−24] The atmospheric transformations may induce visible MIF and MDF of Hg isotopes in PBM,[1] leading to distinguishable isotopic

Received: November 29, 2018
Revised: January 20, 2019
Accepted: January 27, 2019
Published: January 28, 2019

DOI: 10.1021/acs.est.8b06736
Environ. Sci. Technol. 2019, 53, 1947−1957

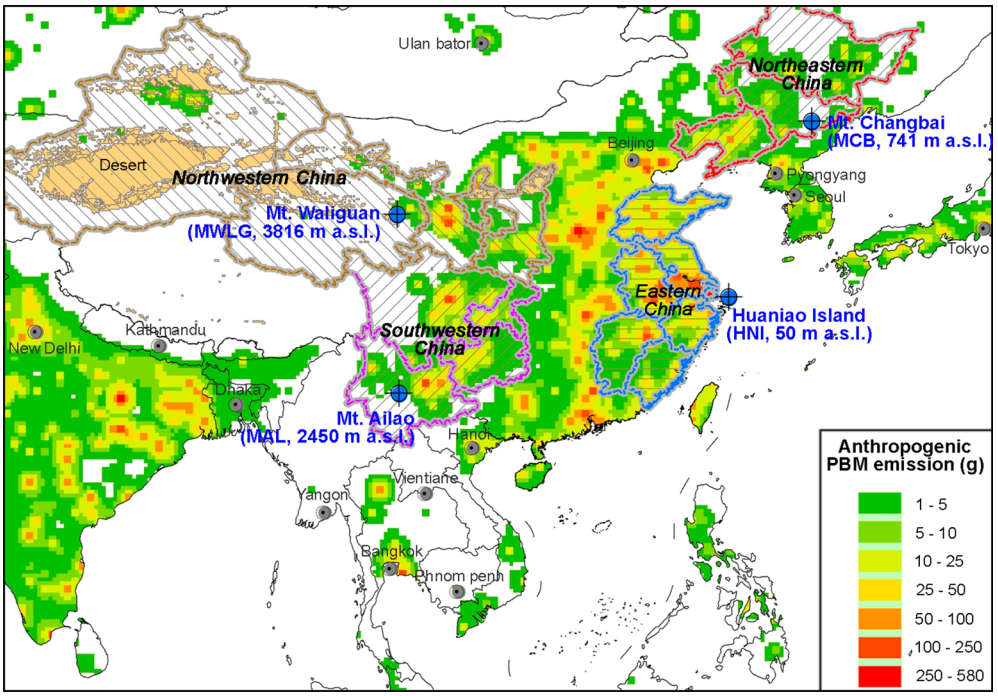

Figure 1. Locations of the four sampling sites in this study, distributions of desert in northwestern China,[56] and gridded anthropogenic PBM emissions in East Asia.[38] The four sampling sites are located in four different geographical regions of China: MWLG in northwestern China (indicated by brown-gray shape), MCB in northeastern China (red-gray shape), MAL in southwestern China (purple-gray shape), and HNI in marine boundary layer of Each China Sea which is close to Eastern China (blue-gray shape).

signatures between background atmospheric pool and direct anthropogenic emissions. However, the influence of atmospheric transformations on PBM isotopic composition has not been investigated. In addition, transformations between PBM and other atmospheric Hg species depend on environmental variables (e.g., photoreduction, air temperature, and atmospheric oxidants), and probably show strong seasonal variations.[22,23] Existing studies on PBM isotopic compositions were conducted at urban sites which were mainly impacted by direct anthropogenic emissions,[19,25,26] or at a semirural site during a very short sampling period (<1 month).[27] To date, no studies have been conducted at background sites and for long enough periods (e.g., covering multiple seasons), limiting our understanding of the temporal and spatial patterns of PBM isotopic compositions and associated controlling factors (e.g., sources and transformations). Such knowledge gaps in PBM isotope composition and fractionation hamper its applications in tracing the cycling of Hg in the atmosphere and many other research areas.

Although only accounting for a small fraction of total Hg in the atmosphere,[28] PBM plays an important role in the global Hg cycling.[22,24] PBM concentrations in East Asia are highly elevated compared to other regions worldwide.[28] To date, however, the sources and atmospheric processes affecting PBM in these regions have not been well constrained. In this study, measurements of PBM isotopic composition were conducted at four remote sites in different geographical regions of China for three to 12 month periods. The major objective of the study was to investigate the temporal and spatial variations in PBM isotopic compositions and associated controlling factors and sources. The PBM isotopic compositions data were further combined with receptor-based model analysis to identify the effects of domestic anthropogenic emissions and transboundary transport on atmospheric PBM pollutions in China.

2. METHODS

2.1. Site Description. Four remote sites from different geographical regions of China were selected for measuring isotopic compositions of PBM (Figure 1 and Supporting Information, SI, Text S1). Briefly, these include two high-altitude sites [Mt. Waliguan Observatory (MWLG) and Mt. Ailao (MAL)], one forested site (Mt. Changbai (MCB)), and one marine boundary layer (MBL) site (Huaniao Island (HNI)). There are no point emission sources around the stations. Prevailing wind direction at MWLG, MCB, MAL, and HNI are from the west and northeast, southwest, southwest, and northwest, respectively. The upwind major anthropogenic PBM source regions for the prevailing wind directions of MWLG, MCB, MAL, and HNI are located approximately 65, 50, 500, and 70 km away from the corresponding sampling sites, respectively (Figure 1).

2.2. Collection, Preconcentration, and Concentration Analysis of Atmospheric PBM. Atmospheric PBM samples were collected onto preheated (500 °C for 6 h) quartz filters (Millipore AQFA 8 × 105, 8 × 10 in. at MWLG, MCB, and HNI and 5 × 8 in. at MAL) using high-volume $PM_{2.5}$ samplers (Shanghai Xintuo Analytical Instruments company) from October 2014 to July 2015 at MWLG, from September 2013 to July 2014 at MCB, from May 2014 to May 2015 at MAL, and from October 2014 to December 2014 at HNI (Table S1). The sampling durations of PBM at MWLG, MCB, and HNI were 96 h, 48−72 h, and 48 h, respectively, at a volumetric flow rate of 1.0 m^3 min^{-1}. The sampling duration of PBM at MAL was 168 h at a volumetric flow rate of 0.3 m^3 min^{-1}.The sampling duration and flow rate were used to collect sufficient atmospheric PBM for isotopic analysis. After field sampling, each quartz filter was folded lengthwise, wrapped with a preheated aluminum foil, sealed with three successive poly-

DOI: 10.1021/acs.est.8b06736
Environ. Sci. Technol. 2019, 53, 1947−1957

ethylene bags and preserved in the refrigerator at a temperature of −18 °C until preconcentration.

PBM collected on quartz filter was preconcentrated into 5−10 mL of 40% mixed acid solution (v/v, $2HNO_3/1HCl$) using a double-stage combustion protocol for Hg isotope analysis as described earlier.[29] Combustion of certified reference material BCR 482 (Lichen, from European Community Bureau of Reference (BCR)) showed a mean recovery of 93.4 ± 2.0% (1σ, $n = 8$).

Hg concentrations in trapping solution were determined using a cold vapor atomic fluorescence spectroscopy (CVAFS), which were further used to calculate the total mass of PBM collected by quartz filters. Atmospheric PBM concentration of each sample was calculated by dividing the total mass of PBM by the total sampling air volume (recorded by high-volume $PM_{2.5}$ samplers). A previous study suggested that the effect of sampling duration on the accuracy of PBM concentration measurement was small in the marine atmosphere.[30] During the sampling of PBM isotope, PBM concentrations were measured simultaneously using the Tekran 2537/1130/1135 system at 1-h resolution at MCB, MAL, and HNI, but not at MWLG. No significant differences in PBM concentrations were observed at MAL or HNI between the two methods (paired sample t test, $p > 0.05$ for both, Table S1). At MCB, mean PBM concentration measured by filters was 20% higher than that measured by the Tekran system (Table S1). The differences in PBM concentrations were possibly caused by adsorption of GOM to filters, loss of Hg due to physical and chemical reactions under dark conditions, or biased low PBM concentrations measured by the Tekran system due to the biased integration of small Hg loads.[30−32] Sampling artifacts of PBM may have a potential to induce measurable shifts in MDF of PBM isotopes but insignificant shift of MIF of PBM isotopes because significant MIF mainly occurs through photochemical reactions.[1]

To ensure clean operation, polyethylene gloves and Teflon tweezers were used throughout the field sampling and laboratory preconcentration. Full procedural blanks of the filed sampling and preconcentration were investigated by combustion of preheated quartz filters. The average procedural blank was 0.04 ± 0.02 ng mL^{-1} (1σ, $n = 7$), which accounted for 0.2−6.9% (mean = 1.6 ± 1.3%, 1σ) of Hg concentrations in trap solutions.

2.3. PBM Isotope Analysis. PBM isotope ratios were measured by Nu-Plasma MC-ICPMS (Nu instruments, U.K.) following the methods described in previous studies.[18,33] Isotopic composition of PBM is reported in delta notation (δ) in per mil (‰) referenced to the bracketed NIST 3133 Hg standard:[34]

$$\delta^{xxx}\mathrm{Hg} = \left(\frac{\left(\frac{^{xxx}\mathrm{Hg}}{^{198}\mathrm{Hg}}\right)_{\mathrm{sample}}}{\left(\frac{^{xxx}\mathrm{Hg}}{^{198}\mathrm{Hg}}\right)_{\mathrm{SRM3133}}} - 1 \right) \times 1000‰ \quad (1)$$

where xxx refers to the mass of each mercury isotope between 199 and 204. MIF values are expressed by "capital delta (Δ)" notation (‰) and calculated using the equations suggested by Blum and Bergquist:[34]

$$\Delta^{199}\mathrm{Hg}(‰) = \delta^{199}\mathrm{Hg} - (0.252 \times \delta^{202}\mathrm{Hg}) \quad (2)$$

$$\Delta^{200}\mathrm{Hg}(‰) = \delta^{200}\mathrm{Hg} - (0.502 \times \delta^{202}\mathrm{Hg}) \quad (3)$$

$$\Delta^{201}\mathrm{Hg}(‰) = \delta^{201}\mathrm{Hg} - (0.752 \times \delta^{202}\mathrm{Hg}) \quad (4)$$

$$\Delta^{204}\mathrm{Hg}(‰) = \delta^{204}\mathrm{Hg} - (1.493 \times \delta^{202}\mathrm{Hg}) \quad (5)$$

Isotopic compositions of standard references UM-Almadén (a secondary standard solution made from metallic Hg mined from Almadén, Spain),[34] NIST 3177 (Mercuric Chloride Standard Solution from National Institute of Standards and Technology (NIST), U.S.A.), and BCR 482 were analyzed repeatedly over different analytical sessions to obtain the analytical uncertainty of isotopic analysis. Overall, measured Hg isotopic compositions of UM-Almadén standard, NIST 3177, and BCR 482 were comparable with previously reported values (Table S2)[6,34,35] The 2σ values on procedural BCR 482 were larger than those of UM-Almadén standard and NIST 3177 (Table S2), similar to what was found in a previous study.[35] The combustion protocol might bring small but detectable analytical uncertainties into the Hg isotopic measurements in this study due to the fractionation of Hg isotopes during combustion and trapping processes given the incomplete and slightly variable extractions of Hg from BCR 482, which might partially explains the higher 2σ value on procedural BCR 482. Analytical uncertainty on Hg isotopic composition in PBM samples was influenced by field sampling, preconcentration process, and instrumental procedures. We unfortunately were not able to measure the analytical uncertainty associated with field sampling. The analytical uncertainty on isotopic composition of BCR 482 was associated with both preconcentration process and instrumental procedures, which is more representative of the true analytical uncertainty of PBM isotopic compositions in this study. Hence, the analytical uncertainty (2σ) of MC-ICPMS isotope analysis reported in this study is the larger 2σ values of either the procedural BCR 482 or the repeated analysis of the sample over different analytical sessions.

2.4. Backward Trajectories of Air Mass and Identification of Potential Source Regions. 120-h backward trajectories of air mass arrived at 300 m height above ground level (a.g.l.), representative of air masses within the boundary layer,[36] at the four sampling sites were calculated every 4 h using the TrajStat Geographical Information System based software and gridded meteorological data (Global Data Assimilation System, GDAS1) from the U.S. National Oceanic and Atmospheric Administration (NOAA).[37] The duration of trajectories was selected to investigate the regional and long-range transport patterns that may have influenced PBM isotopic compositions. To investigate the linkage between atmospheric transport patterns and PBM isotopic compositions, the cumulative anthropogenic PBM emission (∑PBM emission) of each PBM sample was calculated from summing all the gridded emission of the grids encountered by the air mass transported during the preceding 5 days based on the AMAP/UNEP gridded PBM emission inventory in 2010.[38] The ∑PBM emission of each sample was further scaled by different geographic regions to determine the fractional ∑PBM emission over the corresponding geographic regions (i.e., the percentage of ∑PBM emission over a selected geographic region relative to the total of ∑PBM emission). Fractional air mass residence time (ARTs) over ocean and dust regions (i.e., the percentages of ARTs over ocean and dust regions relative to the total of ARTs) were also calculated for each sample regardless of trajectory height, assuming that the effects of these sources on PBM are not limited to the

DOI: 10.1021/acs.est.8b06736
Environ. Sci. Technol. 2019, 53, 1947−1957

atmospheric boundary layer.[39] These pieces of information allowed us to evaluate whether air masses passing over anthropogenic source regions, oceans, and dust regions influenced PBM isotopic compositions.

Potential source regions of PBM at the sampling sites were simulated using a Potential Source Contribution Function (PSCF) modeling.[36,40] The PSCF value in a 1.0° × 1.0° grid cell ($PSCF_{ij}$), indicative of the probability that a source region contributing to elevated atmospheric PBM concentrations (defined by a concentration threshold), is calculated using eq 6:

$$PSCF_{ij} = \frac{M_{ij}}{N_{ij}} W_{ij} \quad (6)$$

where M_{ij} is the total number of trajectory segment end points in a grid cell (ij) related to PBM concentrations above the concentration threshold, N_{ij} is the total number of trajectory segment end points in a grid cell (ij), and W_{ij} is a weighting function used to adjust for a small number of trajectory end points in a grid cell (ij).[2,11] The PSCF analysis needs observations of high-temporal resolution PBM concentrations at receptors. In this study, PBM concentrations at a temporal resolution of 1 h were continuously measured using the Tekran 2537/1130/1135 system at MCB, MAL, and HNI during the sampling periods of the PBM isotope study. High-temporal resolution measurements of PBM concentrations were not conducted during the sampling period of the PBM isotope study at MWLG. Here we use the Tekran PBM concentrations measured from July 2012 to June 2013 to show the potential source regions of PBM at MWLG. Origins of air masses during these two periods were comparable (Figure S1), indicating that the source regions that may have influenced the PBM concentrations at MWLG were similar during the two periods. The concentration thresholds are chosen as the overall median PBM concentrations measured by the Tekran 2537/1130/1135 system at the sampling sites, which are 57.6 pg m^{-3}, 15.0 pg m^{-3}, 22.0 pg m^{-3}, and 15.0 pg m^{-3} at MWLG, MCB, MAL, and HNI, respectively.

We compared the origins of air masses simulated by trajectories with local observed winds and atmospheric wind field in East Asia and tested the sensitivity of fractional ∑PBM emission and fractional ARTs over selected geographical regions as well as the PSCF analysis to trajectory arrival heights (i.e., 300 m a.g.l. versus 100 and 1000 m a.g.l.). All of these comparisons generally showed consistent results (SI Text S2, Figures S2−S4, and Table S3). This indicates that, although associated with uncertainties, it is appropriate to use trajectory-based receptor models for investigating the impact of regional and long-range transport patterns on PBM concentrations and isotopic compositions.

3. RESULTS AND DISCUSSION

3.1. PBM Concentrations. Average (±1σ) atmospheric PBM concentrations measured using quartz filters at MWLG, MCB, MAL, and HNI were 84.5 ± 41.1 pg m^{-3} (n = 25), 22.5 ± 11.1 pg m^{-3} (n = 39), 31.4 ± 29.2 pg m^{-3} (n = 36), and 25.3 ± 15.4 pg m^{-3} (n = 21), respectively (Table S1), which were comparable with those (18.9 to 153 pg m^{-3}) observed at the other remote sites in China but much higher than the global median values (4.6 to 11.0 pg m^{-3}) at rural and remote surface sites and high-elevation sites.[28,41] However, atmospheric PBM concentrations at the four remote sites were lower than those in urban areas of China (mean: 174 to 368 pg m^{-3}) and India (mean: 159 to 408 pg m^{-3}).[26,41]

3.2. PBM Isotopic Compositions. Large variations in MDF and MIF signatures of PBM isotopes were observed at the four sampling sites (Figure S5 and Table S1). In general, PBM samples at the four sites were characterized by significant negative δ^{202}Hg values (means = −1.45 to −0.83‰, n = 4), significant positive Δ^{199}Hg values (mean = 0.27 to 0.66‰, n = 4), and slightly positive Δ^{200}Hg values (mean = 0.07 to 0.10‰, n = 4) (Table S4).

Previous studies on PBM isotopic composition were only conducted at a few sites in Asia and North America. $\delta^{202}Hg_{PBM}$ in this study was comparable to those observed in urban areas of China (mean = −0.71 to −1.26‰, n = 3) and semirural Grand Bay, Mississippi, United States (mean (±1σ) = −0.87 ± 0.48‰),[18,19,25,27,42] but slightly higher than that measured in Kolkata, India (mean (±1σ) = −1.51 ± 0.73‰).[26] Global observations in literatures and this study indicate no significant difference in $\delta^{202}Hg_{PBM}$ between urban (n = 4) and remote sites (n = 5) (Two-independent sample t test, p = 0.67). Mean $\Delta^{199}Hg_{PBM}$ at remotes sites of this study were lower than those measured in semirural Grand Bay, Mississippi, U.S.A. (mean (±1σ) = 0.83 ± 0.35‰),[27] indicating the background PBM pool is characterized by significant positive Δ^{199}Hg. However, mean $\Delta^{199}Hg_{PBM}$ at remotes sites of this study was significantly higher (two-independent sample t test, p < 0.01) than those observed in urban areas of China (mean = −0.02 to 0.05‰, n = 3) and India (mean (±1σ) = −0.04 ± 0.13‰, n = 1).[18,19,25,26] The Δ^{199}Hg signatures of PBM in global urban areas were similar to that of anthropogenic emissions (−0.04‰),[43] suggesting more localized anthropogenic emissions shift the isotopic composition of PBM toward lower Δ^{199}Hg values in urban areas. Mean Δ^{200}Hg of PBM was mostly small positive values at remote and urban sites worldwide (mean = 0.01 to 0.14‰, n = 9).[18,19,25,27]

3.3. Seasonal Variations in PBM Concentrations and Isotopic Compositions. Seasonal variations at HNI were not evaluated since the sampling period was too short. No significant seasonal variations in PBM concentrations were observed at MWLG (K-independent sample t test, p = 0.10). At MCB and MAL, similar seasonal variations in PBM concentrations were observed (K-independent sample t test, p < 0.01 for both) with much higher values in winter (Figure 2 and Table S4). This finding is consistent with many previous studies, which could be explained by increased Hg emissions from wintertime residential heating, increased gas-particle partitioning, reduced wet deposition and photoreduction, and lower mixing height.[22,23,28,41]

Significant seasonal variations in $\Delta^{199}Hg_{PBM}$ were observed at MCB and MAL (K-independent sample t test, p < 0.01 for both, Figure 2), and no significant seasonal variations in $\Delta^{199}Hg_{PBM}$ were observed at MWLG (K-independent sample t test, p = 0.52). At MCB, the highest seasonal mean of $\Delta^{199}Hg_{PBM}$(0.82 ± 0.27‰, ± 1σ) appeared in summer, followed by spring (0.42 ± 0.32‰, ± 1σ) and autumn (0.26 ± 0.19‰, ± 1σ), and the lowest in winter (0.14 ± 0.20‰, ± 1σ) (Table S4). In contrast, the highest seasonal mean appeared in winter (1.05 ± 0.16‰, ± 1σ) at MAL, followed by autumn (0.69 ± 0.23‰, ± 1σ) and spring (0.65 ± 0.20‰, ± 1σ), and the lowest in summer (0.31 ± 0.20‰, ± 1σ) (Table S4). The highest seasonal mean (0.41 ± 0.36‰, ± 1σ) also appeared in winter at MWLG (Table S4). No significant seasonal variations in $\delta^{202}Hg_{PBM}$ were observed at MCB (K-

DOI: 10.1021/acs.est.8b06736
Environ. Sci. Technol. 2019, 53, 1947−1957

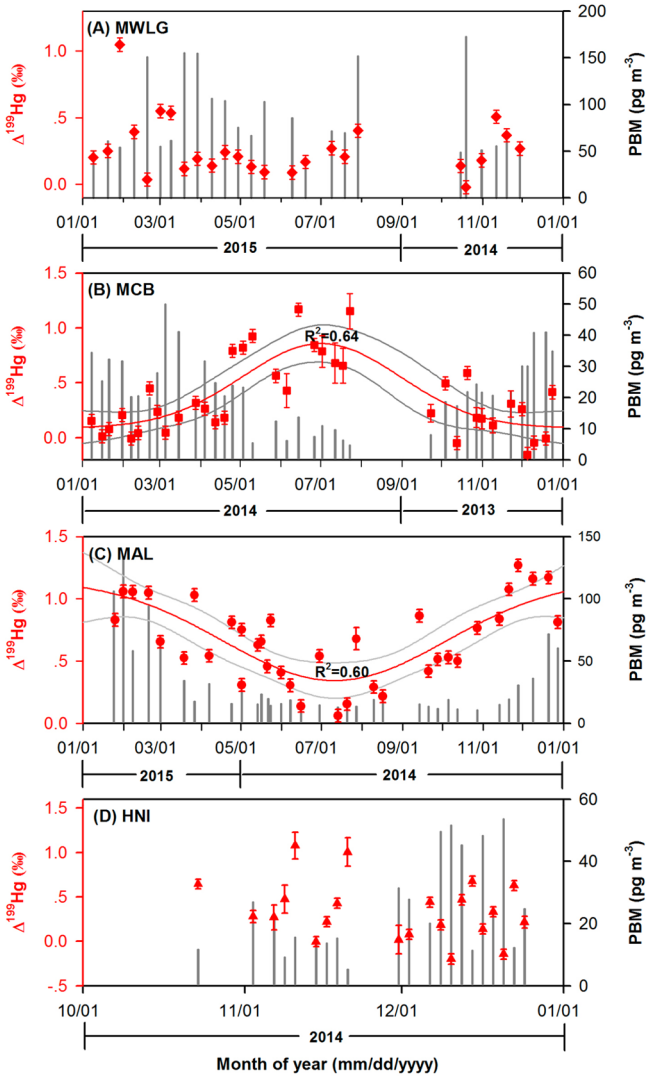

Figure 2. Temporal variations in atmospheric PBM Δ^{199}Hg (red dots) and PBM concentrations (gray vertical bars) at (A) MWLG (Oct 2014 to Jul 2015), (B) MCB (Sep 2014 to Jul 2014), (C) MAL (May 2014 to May 2015), and (D) HNI (Oct 2014 to Dec 2014). The time scales are adjusted for comparing seasonal variability. Error bars are 2σ analytical uncertainty of $\Delta^{199}Hg_{PBM}$. Red lines at MCB and MAL represent the Gaussian regression of data and gray lines are the 95% confidence line of the regression.

independent sample t test, $p = 0.54$) and MAL (K-independent sample t test, $p = 0.56$). A significant seasonal variation in $\delta^{202}Hg_{PBM}$ was observed at MWLG (K-independent sample t test, $p < 0.01$) with much higher values in winter than autumn and spring (Table S4). Air masses at MWLG in winter were exposed to more long-range sources than regional sources, and might undergo more photochemical reactions (e.g., photoreduction) and shift $\delta^{202}Hg_{PBM}$ positively.[3,4]

Significant seasonal variations in $\Delta^{200}Hg_{PBM}$ were observed at MWLG (K-independent sample t test, $p < 0.05$) and MAL (K-independent sample t test, $p < 0.01$) (Figure S6), with seasonal mean being relatively higher in autumn at MWLG and in winter at MAL than in the other seasons (Table S4). No significant seasonal variations were found at MCB (K-independent sample t test, $p = 0.42$, Figure S6). Overall, in northwestern and southwestern China, $\Delta^{199}Hg_{PBM}$ and $\Delta^{200}Hg_{PBM}$ values were generally higher in cold (November to April) than warm season (May to October), whereas an opposite seasonal trend was found in northeastern China (not for $\Delta^{200}Hg_{PBM}$). At MCB, a positive shift of $\Delta^{199}Hg_{PBM}$ in summer was mainly caused by more exposure of air masses to oceanic source (more discussion below), and it is currently unclear whether this source would shift $\Delta^{200}Hg_{PBM}$ positively or negatively.

Isotopic compositions of PBM could be influenced by emission source types as well as transformation processes happened during the short and long-range transport of air pollution. Source materials of anthropogenic origins are generally characterized by much lower Δ^{199}Hg (mean = −0.19‰ to 0.04‰) compared to that of background atmospheric pool.[43] Seasonal variations in industrial Hg emissions are generally small in China. For example, a recent study showed that Hg emission from coal-fired power plants (CFPP) in China was 1−11% higher in winter than in the other seasons.[44] Additionally, there are no notable seasonal variations in the production of cements (<4% higher in summer than in the other seasons) and nonferrous metals (3−5% higher in autumn than in the other seasons) during the last three years.[45] We can therefore assume that industrial emissions in China are kept relatively constant throughout the year with no significant seasonal variations, which could not explain the seasonality in PBM isotopic compositions. Hg emissions from residential coal and wood burning tend to be higher in the cold season due to higher demand for indoor heating.[46] Biomass burning areas, representing the intensity of Hg emissions from biomass burning,[47] in northwestern China, northeastern China, southwest China, and China were generally the highest in spring and the lowest in summer (Figure S7).[48] Analysis of local meteorology shows higher air temperature, solar radiation, and rain depth in the warm season than those in the cold season at all the sampling sites (Figure S8). These factors might partly influence the PBM isotopic compositions observed at individual sites but cannot explain the opposite seasonal trends in $\Delta^{199}Hg_{PBM}$ at MCB and MAL. Therefore, it is speculated that other processes likely dominated the seasonal variations of PBM isotopic compositions.

To investigate the mechanisms driving the seasonal variations in PBM isotopic compositions, we analyzed the atmospheric transport patterns of anthropogenic, oceanic, and dust related sources. Figure S9 shows ∑PBM emission and fractional ∑PBM emission over regional source regions (i.e., northwestern China for MWLG, northeastern China for MCB, southwestern China for MAL, and eastern China for HNI, defined as air masses exposure to regional anthropogenic sources, Figure 1) and major long-range anthropogenic source regions affecting the corresponding sites [i.e., South Asia for MWLG, other regions of China (China excluding northeastern China) for MCB, South Asia for MAL, and other regions of China (China excluding eastern China) for HNI] for each PBM sample at the four sites. ∑PBM emission of PBM samples at each sampling site varied significantly (up to 1 order of magnitude) during the study period (Figure S9). However, no significant relationship existed between $\Delta^{199}Hg_{PBM}$ and ∑PBM emission at MCB, MAL, and HNI (MCB: $r = 0.02$, $p = 0.92$; MAL: $r = 0.22$, $p = 0.20$; HNI: $r = 0.18$, $p = 0.44$). The significant positive correlations at MWLG ($r = 0.67$, $p < 0.01$) was possible owing to the large fraction of ∑PBM emission over long-range source regions, which may shift $\Delta^{199}Hg_{PBM}$

DOI: 10.1021/acs.est.8b06736
Environ. Sci. Technol. 2019, 53, 1947−1957

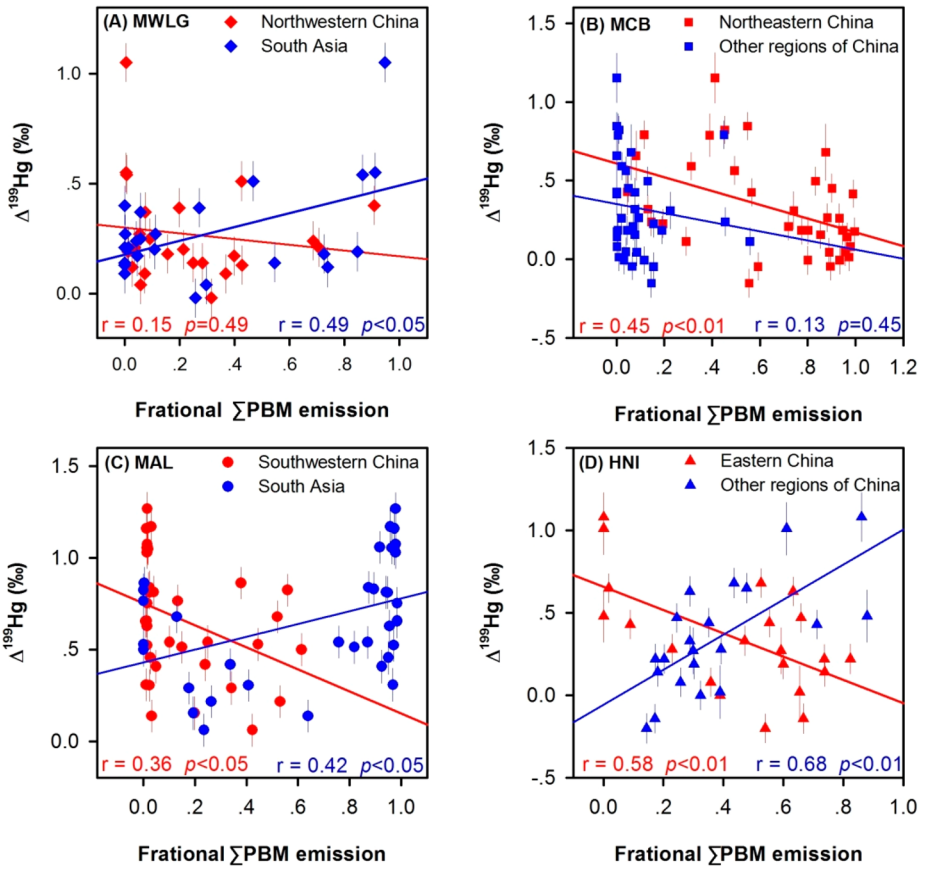

Figure 3. Linear correlation analysis between PBM Δ^{199}Hg and associated fractional ∑PBM emission over regional anthropogenic source regions (i.e., northwestern China for MWLG, northeastern China for MCB, southwestern China for MAL, and eastern China for HNI, indicated by red points) and major long-range anthropogenic source regions [i.e., South Asia for MWLG, other regions of China (China excluding northeastern China) for MCB, South Asia for MAL, and other regions of China (China excluding eastern China) for HNI, indicated by blue points] at (A) MWLG, (B) MCB, (C) MAL, and (D) HNI during the study period. Error bars are 2σ analytical uncertainty of $\Delta^{199}Hg_{PBM}$.

positively during long-range atmospheric transport (more discussion below).

To evaluate the contributions of regional and long-range transport of emissions on PBM isotopic compositions, we analyzed relationships between PBM isotopic compositions ($\Delta^{199}Hg_{PBM}$, $\Delta^{200}Hg_{PBM}$, and $\delta^{202}Hg_{PBM}$) and fractional exposure of air masses to regional sources (e.g., anthropogenic and dust related sources) and long-range sources (e.g., anthropogenic and oceanic sources). We find that air masses with high exposure of the upwind regional anthropogenic sources shifted $\Delta^{199}Hg_{PBM}$ negatively at MCB, MAL, and HNI (Figure 3B–D). At MWLG, $\Delta^{199}Hg_{PBM}$ was not significantly negatively correlated with fractional exposure of air masses to regional anthropogenic sources (Figure 3A), but was significantly negatively correlated with fractional ARTs over the desert region in northwestern China (r = 0.47, p < 0.05, Figure S10), indicating a negative shift of $\Delta^{199}Hg_{PBM}$ by the dust related sources. However, air masses with high exposure of upwind long-range anthropogenic sources shifted $\Delta^{199}Hg_{PBM}$ positively at MWLG, MAL, and HNI (Figure 3A, C, and D). At MCB, a positive shift of $\Delta^{199}Hg_{PBM}$ driven by long-range anthropogenic sources was not observed. It is possibly owing to the overall small fraction of long-range anthropogenic sources (Figure 3B) and indicates other mechanisms might be responsible for the significantly positive $\Delta^{199}Hg_{PBM}$ values observed at MCB. For example, we observed a significant positive correlation between $\Delta^{199}Hg_{PBM}$ and fractional ARTs over oceans at MCB (r = 0.47, p < 0.01, Figure S11), indicating a higher exposure of oceanic air might lead to the positive shift of $\Delta^{199}Hg_{PBM}$. $\Delta^{200}Hg_{PBM}$ at MAL was significantly positively correlated with fractional ∑PBM emission over South Asia (r = 0.44, p < 0.01, Figure S12). $\Delta^{200}Hg_{PBM}$ at HNI was significantly negatively correlated with fractional ∑PBM emission over eastern China (r = 0.65, p < 0.01, Figure S12) and positively correlated with that over the other regions of China (r = 0.57, p < 0.01, Figure S12).

At MCB, the mean fractional ∑PBM emission over northeastern China was 42% in summer (annual mean = 65%) and the mean fractional ARTs over oceans was 33% in summer (annual mean = 14%) (Table S4). At MAL, the mean fractional ∑PBM emission over southwestern China was 2% in winter (annual mean = 15%) and that over South Asia was 95% in winter (annual mean = 66%) (Table S4). At MWLG, the mean fractional ARTs over desert was 14% in winter (annual mean = 17%) and the mean fractional ∑PBM emission over South Asia was 43% in winter (annual mean = 29%) (Table S4). Thus, air masses at MCB in summer and at MWLG and MAL in winter had less exposure to regional sources and more exposure to long-range sources, which could be responsible for the higher $\Delta^{199}Hg_{PBM}$ and $\Delta^{200}Hg_{PBM}$ values in winter at MWLG and MAL and in summer at MCB.

It should be noted that other factors could have also influenced the seasonal variations of the PBM isotopic compositions at the observational sites, resulting in the weak

DOI: 10.1021/acs.est.8b06736
Environ. Sci. Technol. 2019, 53, 1947–1957

correlations between the $\Delta^{199}Hg_{PBM}$ and the PBM transport at some sites (Figure 3). For example, residential heating and biomass burning tend to be intensive in cold seasons in East Asia,[46,48] which might contribute to the low $\Delta^{199}Hg_{PBM}$ values in cold season at MCB. Also, atmospheric transformations including oxidation, reduction, and gas-particle partitioning can shift the isotopic compositions of PBM (more discussion below), which generally have high transformation rates and low partitioning coefficients in warm seasons.[22,23] At MCB, $\Delta^{199}Hg_{PBM}$ was significantly positively correlated with intensity of solar radiation ($r = 0.73$, $p < 0.01$) and air temperature ($r = 0.72$, $p < 0.01$) (Figure S13), indicating meteorologically controlled seasonal variations of $\Delta^{199}Hg_{PBM}$ at MCB. Such correlations, however, were not observed at MWLG and MAL (Figure S13). It is plausible that transport of PBM at MWLG and MAL was a more dominant process than meteorological factors, since the variations of intensity of solar radiation and air temperature at MWLG and MAL were much smaller than that at MCB (Figure S13). $\Delta^{199}Hg_{PBM}$ was negatively correlated with rain depth at MAL ($r = 0.53$, $p < 0.01$, Figure S13). We propose that the frequent rainfall in summer would lead efficient removal of PBM during long-range transport, which in turn increased the impact of regional sources and contributed to the summertime low $\Delta^{199}Hg_{PBM}$ values at MAL.

No significant correlations were observed between $\delta^{202}Hg_{PBM}$ and fractional $\sum$PBM emission over regional anthropogenic source regions and long-range anthropogenic source regions, or between $\delta^{202}Hg_{PBM}$ and fractional ARTs over desert and ocean regions at the four sites (all having p values >0.05, Table S5). $\delta^{202}Hg$ of anthropogenic source materials varied more significantly than $\Delta^{199}Hg$ and $\Delta^{200}Hg$.[43] In addition, unlike that significant MIF is mainly induced by photochemical processes,[1] $\delta^{202}Hg$ signatures of PBM previously emitted from anthropogenic sources could be further shifted by many environmental processes, and it is unclear whether the combined effect of these processes would result in a "net" increase or decrease of $\delta^{202}Hg_{PBM}$.[1] Therefore, currently we are unable to discern the major factors influencing the seasonal variations of $\delta^{202}Hg_{PBM}$.

3.4. Mechanisms for MIF of PBM Isotopes. PBM in the atmosphere could be derived from direct anthropogenic sources or produced via photochemical oxidation of GEM on aerosol surfaces and in gas phase followed by gas-particle partitioning, and removed by photoreduction and deposition.[49] A recent study by Sun et al. compiled Hg isotopic signatures of anthropogenic source materials (e.g., coal, zinc ores, limestone, Hg ores, and volcanic gases) and estimated mean $\Delta^{199}Hg$ values of −0.06 to −0.04‰ and mean $\Delta^{200}Hg$ values of near-zero for PBM and GOM emitted from anthropogenic sources worldwide.[43] This is consistent with the observed $\Delta^{199}Hg_{PBM}$ (mean = −0.02 to 0.05‰) and $\Delta^{200}Hg_{PBM}$ (mean = 0.01 to 0.09‰) in urban areas of Asia,[18,19,25,26] suggesting that strong anthropogenic emissions in urban areas drive isotopic composition of PBM toward low $\Delta^{199}Hg$ and $\Delta^{200}Hg$ values. However, $\Delta^{199}Hg$ and $\Delta^{200}Hg$ values of many PBM samples at remote sites in this study are significantly positive than anthropogenic emissions, indicating important roles of atmospheric transformations.

A recent study on MIF of Hg isotopes during photochemical oxidation of Hg^0 by atomic Cl and Br measured a significant negative shift of $\Delta^{199}Hg$ in GOM products.[6] Therefore, oxidation of Hg^0 followed by gas-particle partitioning of GOM would yield negative $\Delta^{199}Hg$ values in PBM, assuming that temperature-dependent gas-particle partitioning produces insignificant MIF of Hg isotopes.[9,22] In addition, current knowledge of MIF of odd-mass Hg isotopes during Hg evaporation, nonphotochemical reduction, and photoreduction of Hg in snow suggested these processes would probably result in negative or small $\Delta^{199}Hg_{PBM}$ values.[4,5,10] These processes therefore cannot explain the significant positive $\Delta^{199}Hg_{PBM}$ signature in this study. Alternatively, photochemical reduction of Hg(II) in aqueous solution with sulfurless dissolved organic carbon (DOC) can produce a significant positive $\Delta^{199}Hg$ signature in aqueous solution,[3,4] which is consistent with the highly positive $\Delta^{199}Hg_{PBM}$ values commonly observed in remote areas.

The ratio of $\Delta^{199}Hg$ to $\Delta^{201}Hg$ could be also used to identify fractionation processes. In this study, the $\Delta^{199}Hg_{PBM}/\Delta^{201}Hg_{PBM}$ ratios ranged from 1.05 to 1.18 at the four remote sites (Figure S14). These ratios are overall consistent with those of photochemical Hg(II) reduction in aqueous solution with sulfurless DOC (1.00 to 1.31),[3,4] but relatively lower than those observed for gas-phase Hg^0 oxidation by $Cl^•$ and $Br^•$ (1.64 to 1.89), liquid−vapor Hg evaporation (1.59 ± 0.01, 1σ), and abiotic Hg(II) reduction in the absence of light (1.5 to 1.6).[6,50,51] Atmospheric aerosols contain an important fraction of water (30−50% by mass) and DOC (8% by mass),[49,52] and therefore may have similar patterns in photoreduction induced MIF of Hg isotopes as aqueous solutions. Hence, we propose that photoreduction of Hg(II) in aerosols is an important factor driving significant positive $\Delta^{199}Hg_{PBM}$ in background atmospheric pool. It should be noted that PBM in background atmospheric pool could be affected by many environmental processes, and the MIF of Hg isotopes induced by many of these processes have not been well constrained (e.g., photoreduction of gas-phase Hg(II) is supposed to be also important but the MIF of Hg isotopes during this process is unclear[53]). It is plausible that the sum of these processes drive a "net" increase of $\Delta^{199}Hg_{PBM}$ in background atmospheric pool, i.e., processes inducing significant positive shifts of $\Delta^{199}Hg_{PBM}$ dominate over those inducing negative or small shifts.

Interestingly, PBM was mostly characterized by small but significant positive $\Delta^{200}Hg$ values and significant negative $\Delta^{204}Hg$ values in this study. A significant negative correlation was observed between $\Delta^{200}Hg_{PBM}$ and $\Delta^{204}Hg_{PBM}$ at MWLG and MAL ($\Delta^{204}Hg_{PBM}$ was not measured at MCB and HNI due to the limitations of instrumental collector designs during that analytical sessions) and yielded a $\Delta^{200}Hg_{PBM}/^{204}Hg_{PBM}$ slope of −0.54 (Figure S15), which is comparable to previous studies.[2,15] Significant MIF of even-mass Hg isotopes has been mainly observed in atmospheric samples, generally with negative $\Delta^{200}Hg$ in GEM and positive $\Delta^{200}Hg$ in PBM, GOM and precipitation.[12,14−16,27] The unique $\Delta^{200}Hg$ anomalies in atmospheric Hg samples have been suggested to be mainly related to photochemical oxidation of Hg^0 at high altitudes (e.g., upper troposphere and stratosphere where UV-light and oxidants are abundant).[2,12] Here we analyzed the air mass origins of the high $\Delta^{200}Hg_{PBM}$ events (i.e., $\Delta^{200}Hg_{PBM} \geq 0.15$‰, $n = 13$). As shown in Figure S16, air masses related to high $\Delta^{200}Hg_{PBM}$ events at MCB ($n = 5$) mainly originated from the middle and upper troposphere (e.g., > 3 km a.g.l.) over high-latitude regions and passed over lower free troposphere (1−3 km a.g.l.) before arriving at MCB during the preceding 5 days. However, air masses related to high $\Delta^{200}Hg_{PBM}$ events at HNI ($n = 2$) and MAL ($n = 6$) showed major origins and pathways at the low altitudes (e.g., lower free troposphere and

DOI: 10.1021/acs.est.8b06736
Environ. Sci. Technol. 2019, 53, 1947−1957

MBL) during the preceding 5 days (Figure S16). This may not support the hypothesis that intrusion of air mass from upper troposphere and stratosphere directly causes Δ^{200}Hg anomalies in ground atmospheric PBM. It is speculated that small but significant Δ^{200}Hg anomalies might be a widespread phenomenon in the background global atmospheric PBM pool, which could be originated from vertical mixing of air masses between the stratosphere and the troposphere,[54] and/or in situ photochemical oxidation of Hg^0 by UV light and oxidants (e.g., $Cl^•$) at low altitudes.[6]

3.5. Domestic versus Transboundary Air Pollution Contributing to Atmospheric PBM. Atmospheric PBM concentrations were significantly negatively correlated with $\Delta^{199}Hg_{PBM}$ at MCB and HNI (MCB: $r = 0.62$, $p < 0.01$; HNI: $r = 0.66$, $p < 0.01$) and significantly positively correlated at MAL ($r = 0.47$, $p < 0.01$) (Figure 4). No significant

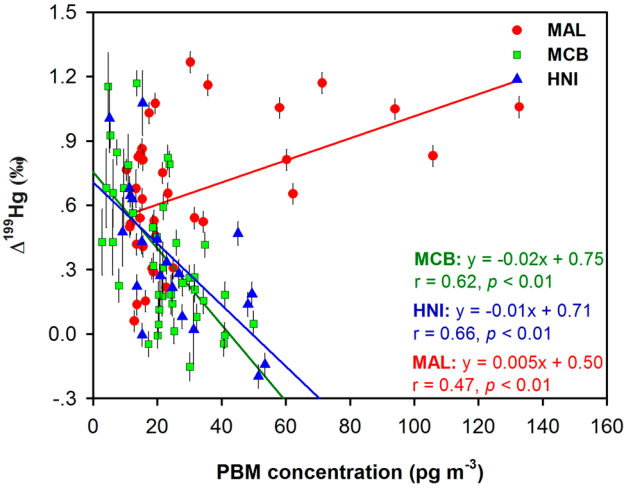

Figure 4. Linear relationships between PBM concentration and PBM Δ^{199}Hg at MAL, MCB, and HNI. Error bars are 2σ analytical uncertainty of $\Delta^{199}Hg_{PBM}$.

relationship existed between PBM concentrations and $\Delta^{199}Hg_{PBM}$ at MWLG ($r = 0.39$, $p = 0.06$). The different relationships between PBM concentrations and Δ^{199}Hg indicate different sources of atmospheric PBM between the studied sites. At MCB and HNI, PBM samples with elevated concentrations were mainly associated with low $\Delta^{199}Hg_{PBM}$ values, similar to the Δ^{199}Hg signatures of direct anthropogenic emissions,[43] suggesting major contributions from this category of sources to PBM at these two sites. However, low atmospheric PBM concentrations at the same two sites were mainly associated with significantly positive $\Delta^{199}Hg_{PBM}$ values. PBM in the background atmospheric pool (e.g., lower free troposphere and grounded remote areas) is generally low (e.g., 4−11 pg m),[28] and undergoes sufficient atmospehric transformations that probably drives PBM isotopic composition toward significantly positive Δ^{199}Hg values. Additionally, sufficient photochemical reductions of PBM previously emitted from anthropogenic sources during long-range transport could also decrease PBM concentrations and increase $\Delta^{199}Hg_{PBM}$ values.

Contrary to the cases found at MCB and HNI, elevated atmospheric PBM concentrations (e.g., 58.1 to 132.7 pg m^{-3}, $n = 7$) at MAL were mainly associated with significantly positive $\Delta^{199}Hg_{PBM}$ (0.65 to 1.17‰) (Figure 4), which cannot be explained by the commonly observed low PBM concentrations in the background atmospheric pool.[28] It is speculated that long-range transport of anthropogenic pollution plumes that underwent strong atmospheric transformations contributed significantly to the elevated PBM at MAL. Low atmospheric PBM at MAL was associated with a large range (from low to significantly positive) of $\Delta^{199}Hg_{PBM}$ values, suggesting combined contributions from direct anthropogenic emissions and background PBM pool.

Source regions of the elevated PBM at the studied sites are identified using a PSCF approach. Major potential source regions at MCB and HNI were mainly located in the planetary boundary layer (PBL) over northeastern China and eastern China, respectively (Figures 5B and D and S17), corresponding well with the major anthropogenic source regions in China (Figure 1). These sources can be classified to regional sources because of the proximity of these sources to MCB and HNI. PBM emitted from these source regions could be transported to these two sites within a short time period (e.g., 0−48 h, Figure S18). Such a short transport period and a major transport pathway within the PBL are not expected to cause strong transformations of PBM, leading the Δ^{199}Hg signatures of the elevated PBM similar to that of the original anthropogenic sources. In comparison, elevated PBM at MAL were mainly attributed to the transboundary transport of PBM from the lower free troposphere (2−3 km a.g.l.) over South Asia (Figures 5C and S17). A recent study in urbanized and industrialized Kolkata, Northeast India reported highly elevated PBM concentrations (159 to 408 pg m^{-3}) and close to zero $\Delta^{199}Hg_{PBM}$ values.[26] Anthropogenic pollution plumes from South Asia needed to travel a longer period (48−120 h) in the lower free troposphere (2−3 km altitude) before arriving at MAL (Figures S17 and S18). A modeling study estimated that the global mean chemical lifetime of Hg(II) against photoreduction in aerosols and clouds in the troposphere is approximately 13 days.[24] It is probably much shorter in Asian lower free troposphere (1−2 km altitude) because of higher organic aerosols concentrations.[23,24] This indicates that more than 15−38% of the PBM from South Asia was lost via photoreduction during long-range transport, which likely drove a notable positive shift of $\Delta^{199}Hg_{PBM}$ given the dramatic MIF factors induced by photochemical reduction as determined by previous experiments.[3,4] Identification of potential source regions at MWLG reflected mixing sources between dust related emissions over desert and semidesert regions in western China and a transboundary transport from northwestern South Asia (Figure 5A). Fractional ∑PBM emission over South Asia was significantly positively correlated with $\Delta^{199}Hg_{PBM}$ at MWLG (Figure 3A), similar to what was found at MAL, indicating transboundary transport also played an important role at MWLG.

3.6. Environmental Implications. Strong anthropogenic Hg emissions combined with high particulate matter (PM) concentrations enhanced Hg(II) gas-particle partitioning[22,55] and resulted in elevated atmospheric PBM concentrations in East Asia.[28] Our analysis suggests that exposure of air masses to regional and long-range sources in the preceding days had distinct MIF signatures of PBM isotopes. Due to the proximity to the sampling sites, PBM emitted from regional anthropogenic and dust related sources could be transported to the receptors within short time periods and might conserve the low Δ^{199}Hg signatures of the original sources.[43] In contrast, long-range transported PBM of anthropogenic or oceanic origins underwent more atmospheric transformations and/or mixed

DOI: 10.1021/acs.est.8b06736
Environ. Sci. Technol. 2019, 53, 1947−1957

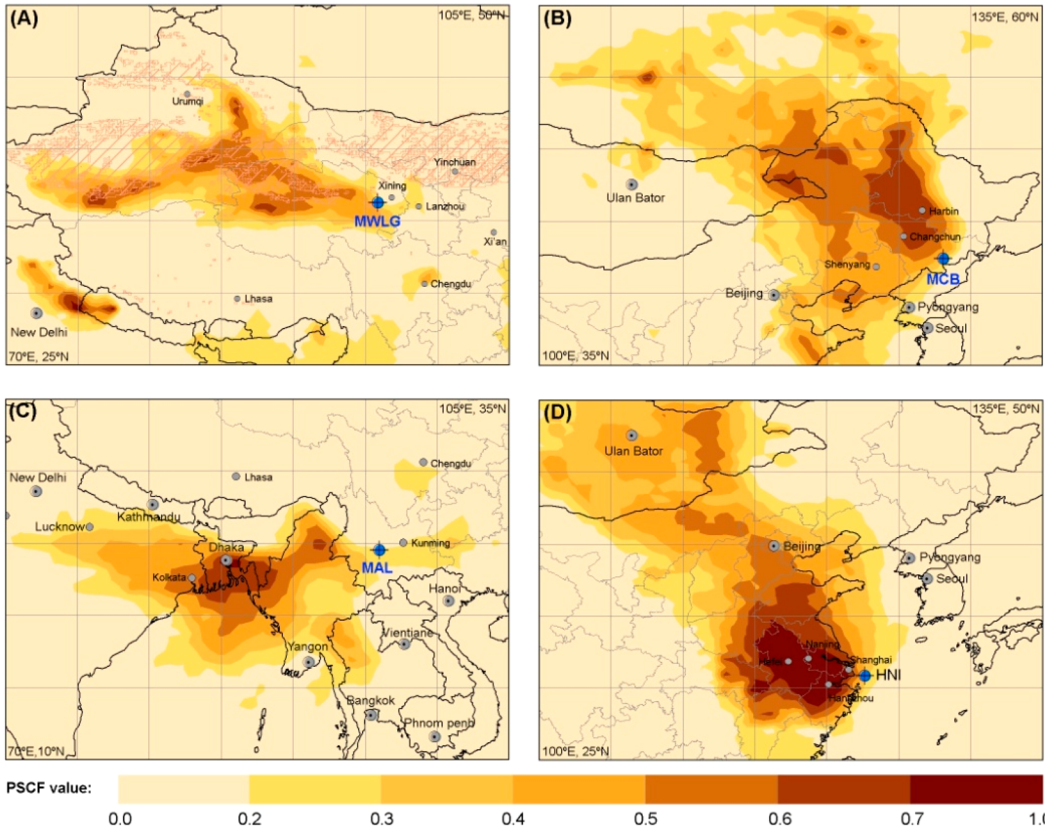

Figure 5. Identified potential source regions of atmospheric PBM at (A) MWLG, (B) MCB, (C) MAL, and (D) HNI. Areas with high PSCF values have a higher probability contributing to elevated PBM concentrations at the sampling sites.

with PBM produced via atmospheric processes, and probably shifted the MIF signatures of PBM isotopes positively relative to the original isotope signatures. This finding suggests that the $\Delta^{199}Hg_{PBM}$ signature would be a potential tracer in identifying PBM source factors, despite the fact that the potential mechanisms driving the significant positive $\Delta^{199}Hg_{PBM}$ signatures are still not well understood. Future studies are needed to better understand the transformation induced fractionation of Hg isotopes in atmospheric PBM. This, together with the established isotopic compositions of anthropogenic sources,[43] would help to quantitatively identify the sources of atmospheric PBM. Such knowledge is also needed in assessing the influence of the fractionation of PBM isotopes on isotopic compositions of Hg in other atmospheric reservoirs.

■ ASSOCIATED CONTENT

Supporting Information

The Supporting Information is available free of charge on the ACS Publications website at DOI: 10.1021/acs.est.8b06736.

Additional information on the sampling sites, atmospheric PBM concentrations and isotopic compositions, backward trajectories, fractional ∑PBM emission and fractional atmospheric ARTs over selected geographical regions, and ancillary observations and modeling results (Figures S1−S18 and Tables S1−S5) (PDF)

■ AUTHOR INFORMATION

Corresponding Authors

*Tel:+86 851 85891508; fax: +86 851 85891609; e-mail: fuxuewu@mail.gyig.ac.cn.

*Tel:+86 851 85891356; fax: +86 851 85891609; e-mail: fengxinbin@vip.skleg.cn.

ORCID

Xuewu Fu: 0000-0002-5174-7150

Xinbin Feng: 0000-0002-7462-8998

Leiming Zhang: 0000-0001-5437-5412

Notes

The authors declare no competing financial interest.

■ ACKNOWLEDGMENTS

This work was funded by the National Science Foundation of China (41622305), the Strategic Priority Research Program of Chinese Academy of Sciences, Pan-Third Pole Environment Study for a Green Silk Road (Pan-TPE, XDA20040502), the CAS "Light of West China" program, the CAS Youth Innovation Promotion Association (2017443), and the K.C. Wong Education Foundation.

■ REFERENCES

(1) Blum, J. D.; Sherman, L. S.; Johnson, M. W. Mercury isotopes in earth and environmental sciences. *Annu. Rev. Earth Planet. Sci.* **2014**, *42*, 249−269.

(2) Blum, J. D.; Johnson, M. W. Recent Developments in Mercury Stable Isotope Analysis. *Rev. Mineral. Geochem.* **2017**, *82*, 733−757.

(3) Bergquist, B. A.; Blum, J. D. Mass-dependent and -independent fractionation of Hg isotopes by photoreduction in aquatic systems. *Science* **2007**, *318* (5849), 417−420.

DOI: 10.1021/acs.est.8b06736
Environ. Sci. Technol. 2019, 53, 1947−1957

(4) Zheng, W.; Hintelmann, H. Mercury isotope fractionation during photoreduction in natural water is controlled by its Hg/DOC ratio. *Geochim. Cosmochim. Acta* **2009**, *73* (22), 6704−6715.
(5) Sherman, L. S.; Blum, J. D.; Johnson, K. P.; Keeler, G. J.; Barres, J. A.; Douglas, T. A. Mass-independent fractionation of mercury isotopes in Arctic snow driven by sunlight. *Nat. Geosci.* **2010**, *3* (3), 173−177.
(6) Sun, G.; Sommar, J.; Feng, X.; Lin, C.-J.; Ge, M.; Wang, W.; Yin, R.; Fu, X.; Shang, L. Mass-dependent and -independent fractionation of mercury isotope during gas-phase oxidation of elemental mercury vapor by atomic Cl and Br. *Environ. Sci. Technol.* **2016**, *50* (17), 9232−9241.
(7) Kritee, K.; Barkay, T.; Blum, J. D. Mass dependent stable isotope fractionation of mercury during *mer* mediated microbial degradation of monomethylmercury. *Geochim. Cosmochim. Acta* **2009**, *73* (5), 1285−1296.
(8) Rodriguez-Gonzalez, P.; Epov, V. N.; Bridou, R.; Tessier, E.; Guyoneaud, R.; Monperrus, M.; Amouroux, D. Species-Specific Stable Isotope Fractionation of Mercury during Hg(II) Methylation by an Anaerobic Bacteria (Desulfobulbus propionicus) under Dark Conditions. *Environ. Sci. Technol.* **2009**, *43* (24), 9183−9188.
(9) Wiederhold, J. G.; Cramer, C. J.; Daniel, K.; Infante, I.; Bourdon, B.; Kretzschmar, R. Equilibrium Mercury Isotope Fractionation between Dissolved Hg(II) Species and Thiol-Bound Hg. *Environ. Sci. Technol.* **2010**, *44* (11), 4191−4197.
(10) Estrade, N.; Carignan, J.; Sonke, J. E.; Donard, O. F. X. Mercury isotope fractionation during liquid-vapor evaporation experiments. *Geochim. Cosmochim. Acta* **2009**, *73* (10), 2693−2711.
(11) Zheng, W.; Foucher, D.; Hintelmann, H. Mercury isotope fractionation during volatilization of Hg(0) from solution into the gas phase. *J. Anal. At. Spectrom.* **2007**, *22* (9), 1097−1104.
(12) Chen, J. B.; Hintelmann, H.; Feng, X. B.; Dimock, B. Unusual fractionation of both odd and even mercury isotopes in precipitation from Peterborough, ON, Canada. *Geochim. Cosmochim. Acta* **2012**, *90*, 33−46.
(13) Mead, C.; Lyons, J. R.; Johnson, T. M.; Anbar, A. D. Unique Hg Stable Isotope Signatures of Compact Fluorescent Lamp-Sourced Hg. *Environ. Sci. Technol.* **2013**, *47* (6), 2542−2547.
(14) Gratz, L. E.; Keeler, G. J.; Blum, J. D.; Sherman, L. S. Isotopic composition and fractionation of mercury in Great Lakes precipitation and ambient air. *Environ. Sci. Technol.* **2010**, *44* (20), 7764−7770.
(15) Demers, J. D.; Blum, J. D.; Zak, D. R. Mercury isotopes in a forested ecosystem: Implications for air-surface exchange dynamics and the global mercury cycle. *Global Biogeochem Cy* **2013**, *27* (1), 222−238.
(16) Demers, J. D.; Sherman, L. S.; Blum, J. D.; Marsik, F. J.; Dvonch, J. T. Coupling atmospheric mercury isotope ratios and meteorology to identify sources of mercury impacting a coastal urban-industrial region near Pensacola, Florida, USA. *Global Biogeochem Cy* **2015**, *29* (10), 1689−1705.
(17) Fu, X. W.; Marusczak, N.; Wang, X.; Gheusi, F.; Sonke, J. E. Isotopic Composition of Gaseous Elemental Mercury in the Free Troposphere of the Pic du Midi Observatory, France. *Environ. Sci. Technol.* **2016**, *50* (11), 5641−5650.
(18) Yu, B.; Fu, X.; Yin, R.; Zhang, H.; Wang, X.; Lin, C.-J.; Wu, C.; Zhang, Y.; He, N.; Fu, P.; Wang, Z.; Shang, L.; Sommar, J.; Sonke, J. E.; Maurice, L.; Guinot, B.; Feng, X. Isotopic Composition of Atmospheric Mercury in China: New Evidence for Sources and Transformation Processes in Air and in Vegetation. *Environ. Sci. Technol.* **2016**, *50* (17), 9262−9269.
(19) Xu, H.; Sonke, J. E.; Guinot, B.; Fu, X.; Sun, R.; Lanzanova, A.; Candaudap, F.; Shen, Z.; Cao, J. Seasonal and Annual Variations in Atmospheric Hg and Pb Isotopes in Xi'an, China. *Environ. Sci. Technol.* **2017**, *51* (7), 3759−3766.
(20) Fu, X.; Yang, X.; Tan, Q.; Ming, L.; Lin, T.; Lin, C.-J.; Li, X.; Feng, X. Isotopic Composition of Gaseous Elemental Mercury in the Marine Boundary Layer of East China Sea. *Journal of Geophysical Research: Atmospheres* **2018**, *123* (14), 7656−7669.
(21) Obrist, D.; Agnan, Y.; Jiskra, M.; Olson, C. L.; Colegrove, D. P.; Hueber, J.; Moore, C. W.; Sonke, J. E.; Helmig, D. Tundra uptake of atmospheric elemental mercury drives Arctic mercury pollution. *Nature* **2017**, *547* (7662), 201−204.
(22) Amos, H. M.; Jacob, D. J.; Holmes, C. D.; Fisher, J. A.; Wang, Q.; Yantosca, R. M.; Corbitt, E. S.; Galarneau, E.; Rutter, A. P.; Gustin, M. S.; Steffen, A.; Schauer, J. J.; Graydon, J. A.; St Louis, V. L.; Talbot, R. W.; Edgerton, E. S.; Zhang, Y.; Sunderland, E. M. Gas-particle partitioning of atmospheric Hg(II) and its effect on global mercury deposition. *Atmos. Chem. Phys.* **2012**, *12* (1), 591−603.
(23) Holmes, C. D.; Jacob, D. J.; Corbitt, E. S.; Mao, J.; Yang, X.; Talbot, R.; Slemr, F. Global atmospheric model for mercury including oxidation by bromine atoms. *Atmos. Chem. Phys.* **2010**, *10* (24), 12037−12057.
(24) Horowitz, H. M.; Jacob, D. J.; Zhang, Y. X.; Dibble, T. S.; Slemr, F.; Amos, H. M.; Schmidt, J. A.; Corbitt, E. S.; Marais, E. A.; Sunderland, E. M. A new mechanism for atmospheric mercury redox chemistry: implications for the global mercury budget. *Atmos. Chem. Phys.* **2017**, *17* (10), 6353−6371.
(25) Huang, Q.; Chen, J. B.; Huang, W. L.; Fu, P. Q.; Guinot, B.; Feng, X. B.; Shang, L. H.; Wang, Z. H.; Wang, Z. W.; Yuan, S. L.; Cai, H. M.; Wei, L. F.; Yu, B. Isotopic composition for source identification of mercury in atmospheric fine particles. *Atmos. Chem. Phys.* **2016**, *16* (18), 11773−11786.
(26) Das, R.; Wang, X. F.; Khezri, B.; Webster, R. D.; Sikdar, P. K.; Datta, S. Mercury isotopes of atmospheric particle bound mercury for source apportionment study in urban Kolkata, India. *Elementa-Sci. Anthrop* **2016**, *4*, 1−12.
(27) Rolison, J. M.; Landing, W. M.; Luke, W.; Cohen, M.; Salters, V. J. M. Isotopic composition of species-specific atmospheric Hg in a coastal environment. *Chem. Geol.* **2013**, *336*, 37−49.
(28) Mao, H. T.; Cheng, I.; Zhang, L. M. Current understanding of the driving mechanisms for spatiotemporal variations of atmospheric speciated mercury: a review. *Atmos. Chem. Phys.* **2016**, *16* (20), 12897−12924.
(29) Huang, Q.; Liu, Y. L.; Chen, J. B.; Feng, X. B.; Huang, W. L.; Yuan, S. L.; Cai, H. M.; Fu, X. W. An improved dual-stage protocol to pre-concentrate mercury from airborne particles for precise isotopic measurement. *J. Anal. At. Spectrom.* **2015**, *30* (4), 957−966.
(30) Malcolm, E. G.; Keeler, G. J. Evidence for a sampling artifact for particulate-phase mercury in the marine atmosphere. *Atmos. Environ.* **2007**, *41* (16), 3352−3359.
(31) Talbot, R.; Mao, H. T.; Feddersen, D.; Smith, M.; Kim, S. Y.; Sive, B.; Haase, K.; Ambrose, J.; Zhou, Y.; Russo, R. Comparison of Particulate Mercury Measured with Manual and Automated Methods. *Atmosphere* **2011**, *2* (1), 1−20.
(32) Ambrose, J. L. Improved methods for signal processing in measurements of mercury by Tekran (R) 2537A and 2537B instruments. *Atmos. Meas. Tech.* **2017**, *10* (12), 5063−5073.
(33) Yin, R. S.; Feng, X. B.; Foucher, D.; Shi, W. F.; Zhao, Z. Q.; Wang, J. High Precision Determination of Mercury Isotope Ratios Using Online Mercury Vapor Generation System Coupled with Multi-collector Inductively Coupled Plasma-Mass Spectrometry. *Chinese J. Anal Chem.* **2010**, *38* (7), 929−934.
(34) Blum, J. D.; Bergquist, B. A. Reporting of variations in the natural isotopic composition of mercury. *Anal. Bioanal. Chem.* **2007**, *388* (2), 353−359.
(35) Estrade, N.; Carignan, J.; Sonke, J. E.; Donard, O. F. X. Measuring Hg Isotopes in Bio-Geo-Environmental Reference Materials. *Geostand. Geoanal. Res.* **2010**, *34* (1), 79−93.
(36) Cheng, I.; Xu, X.; Zhang, L. Overview of receptor-based source apportionment studies for speciated atmospheric mercury. *Atmos. Chem. Phys.* **2015**, *15* (14), 7877−7895.
(37) Wang, Y. Q.; Zhang, X. Y.; Draxler, R. R. TrajStat: GIS-based software that uses various trajectory statistical analysis methods to identify potential sources from long-term air pollution measurement data. *Environ. Modell Softw* **2009**, *24* (8), 938−939.
(38) AMAP/UNEP, Geospatially distributed mercury emissions dataset 2010v1. In 2013.

DOI: 10.1021/acs.est.8b06736
Environ. Sci. Technol. 2019, 53, 1947−1957

(39) Zhou, T.; Xie, H. L.; Bi, J. R.; Huang, Z. W.; Huang, J. P.; Shi, J. S.; Zhang, B. D.; Zhang, W. Lidar Measurements of Dust Aerosols during Three Field Campaigns in 2010, 2011, and 2012 over Northwestern China. *Atmosphere* **2018**, *9* (5), 173
(40) Fu, X. W.; Feng, X.; Shang, L. H.; Wang, S. F.; Zhang, H. Two years of measurements of atmospheric total gaseous mercury (TGM) at a remote site in Mt. Changbai area, Northeastern China. *Atmos. Chem. Phys.* **2012**, *12* (9), 4215−4226.
(41) Fu, X. W.; Zhang, H.; Yu, B.; Wang, X.; Lin, C. J.; Feng, X. B. Observations of atmospheric mercury in China: a critical review. *Atmos. Chem. Phys.* **2015**, *15* (16), 9455−9476.
(42) Huang, S. Y.; Sun, L. M.; Zhou, T. J.; Yuan, D. X.; Du, B.; Sun, X. W. Natural stable isotopic compositions of mercury in aerosols and wet precipitations around a coal-fired power plant in Xiamen, southeast China. *Atmos. Environ.* **2018**, *173*, 72−80.
(43) Sun, R. Y.; Streets, D. G.; Horowitz, H. M.; Amos, H. M.; Liu, G. J.; Perrot, V.; Toutain, J. P.; Hintelmann, H.; Sunderland, E. M.; Sonke, J. E. Historical (1850−2010) mercury stable isotope inventory from anthropogenic sources to the atmosphere. *Elem. Sci. Anth* **2016**, *4* (91), 000091
(44) Liu, K. Y.; Wang, S. X.; Wu, Q. R.; Wang, L.; Ma, Q.; Zhang, L.; Li, G. L.; Tian, H. Z.; Duan, L.; Hao, J. M. A Highly Resolved Mercury Emission Inventory of Chinese Coal-Fired Power Plants. *Environ. Sci. Technol.* **2018**, *52* (4), 2400−2408.
(45) National Bureau of Statistics of China, P. R. C. http://data.stats.gov.cn/english/.
(46) Feng, X. B.; Shang, L. H.; Wang, S. F.; Tang, S. L.; Zheng, W. Temporal variation of total gaseous mercury in the air of Guiyang, China. *J. Geophys. Res.-Atmos.* **2004**, *109* (D3) DOI: 10.1029/2003JD004159.
(47) Friedli, H. R.; Arellano, A. F.; Cinnirella, S.; Pirrone, N. Initial Estimates of Mercury Emissions to the Atmosphere from Global Biomass Burning. *Environ. Sci. Technol.* **2009**, *43* (10), 3507−3513.
(48) Giglio, L.; Randerson, J. T.; van der Werf, G. R. Analysis of daily, monthly, and annual burned area using the fourth-generation global fire emissions database (GFED4). *J. Geophys. Res.: Biogeosci.* **2013**, *118* (1), 317−328.
(49) Ariya, P. A.; Amyot, M.; Dastoor, A.; Deeds, D.; Feinberg, A.; Kos, G.; Poulain, A.; Ryjkov, A.; Semeniuk, K.; Subir, M.; Toyota, K. Mercury Physicochemical and Biogeochemical Transformation in the Atmosphere and at Atmospheric Interfaces: A Review and Future Directions. *Chem. Rev.* **2015**, *115* (10), 3760−3802.
(50) Ghosh, S.; Schauble, E. A.; Couloume, G. L.; Blum, J. D.; Bergquist, B. A. Estimation of nuclear volume dependent fractionation of mercury isotopes in equilibrium liquid-vapor evaporation experiments. *Chem. Geol.* **2013**, *336*, 5−12.
(51) Zheng, W.; Hintelmann, H. Nuclear Field Shift Effect in Isotope Fractionation of Mercury during Abiotic Reduction in the Absence of Light. *J. Phys. Chem. A* **2010**, *114* (12), 4238−4245.
(52) Gioda, A.; Reyes-Rodriguez, G. J.; Santos-Figueroa, G.; Collett, J. L.; Decesari, S.; Ramos, M. D. K. V.; Netto, H. J. C. B.; Neto, F. R. d. A.; Mayol-Bracero, O. L. Speciation of water-soluble inorganic, organic, and total nitrogen in a background marine environment: Cloud water, rainwater, and aerosol particles. *J. Geophys. Res.* **2011**, *116* DOI: 10.1029/2010JD015010.
(53) Saiz-Lopez, A.; Sitkiewicz, S. P.; Roca-Sanjuan, D.; Oliva-Enrich, J. M.; Davalos, J. Z.; Notario, R.; Jiskra, M.; Xu, Y.; Wang, F.; Thackray, C. P.; Sunderland, E. M.; Jacob, D. J.; Travnikov, O.; Cuevas, C. A.; Acuna, A. U.; Rivero, D.; Plane, J. M. C.; Kinnison, D. E.; Sonke, J. E. Photoreduction of gaseous oxidized mercury changes global atmospheric mercury speciation, transport and deposition. *Nat. Commun.* **2018**, *9* DOI: 10.1038/s41467-018-07075-3.
(54) Seo, K. H.; Bowman, K. P. Lagrangian estimate of global stratosphere-troposphere mass exchange. *J. Geophys Res.-Atmos.* **2002**, *107* (D21), ACL2-1.
(55) Zhang, L.; Wang, S. X.; Wang, L.; Wu, Y.; Duan, L.; Wu, Q. R.; Wang, F. Y.; Yang, M.; Yang, H.; Hao, J. M.; Liu, X. Updated Emission Inventories for Speciated Atmospheric Mercury from Anthropogenic Sources in China. *Environ. Sci. Technol.* **2015**, *49* (5), 3185−3194.
(56) Zhang, X. Y.; Gong, S. L.; Zhao, T. L.; Arimoto, R.; Wang, Y. Q.; Zhou, Z. J. Sources of Asian dust and role of climate change versus desertification in Asian dust emission. *Geophys. Res. Lett.* **2003**, *30* (24) DOI: 10.1029/2003GL018206.

DOI: 10.1021/acs.est.8b06736
Environ. Sci. Technol. 2019, 53, 1947−1957